

# Migration of Zebrafish Primordial Germ Cells: A Role for Myosin Contraction and Cytoplasmic Flow

Heiko Blaser,<sup>1,5</sup> Michal Reichman-Fried,<sup>1,5</sup>  
Irinka Castanon,<sup>2</sup> Karin Dumstrei,<sup>1</sup>  
Florence L. Marlow,<sup>3,6</sup> Koichi Kawakami,<sup>4</sup>  
Lilianna Solnica-Krezel,<sup>3</sup> Carl-Philipp Heisenberg,<sup>2</sup>  
and Erez Raz<sup>1,\*</sup>

<sup>1</sup> Germ Cell Development

Max Planck Institute for Biophysical Chemistry  
Am Fassberg 11  
37077 Göttingen  
Germany

<sup>2</sup> Max Planck Institute of Molecular Cell Biology  
and Genetics

Pfotenhauerstr. 108  
01307 Dresden  
Germany

<sup>3</sup> Department of Biological Sciences

Vanderbilt University  
Nashville, Tennessee 37235

<sup>4</sup> Division of Molecular and Developmental Biology

National Institute of Genetics

1111 Yata, Mishima  
Shizuoka 411-8540

Japan

## Summary

The molecular and cellular mechanisms governing cell motility and directed migration in response to the chemokine SDF-1 are largely unknown. Here, we demonstrate that zebrafish primordial germ cells whose migration is guided by SDF-1 generate bleb-like protrusions that are powered by cytoplasmic flow. Protrusions are formed at sites of higher levels of free calcium where activation of myosin contraction occurs. Separation of the acto-myosin cortex from the plasma membrane at these sites is followed by a flow of cytoplasm into the forming bleb. We propose that polarized activation of the receptor CXCR4 leads to a rise in free calcium that in turn activates myosin contraction in the part of the cell responding to higher levels of the ligand SDF-1. The biased formation of new protrusions in a particular region of the cell in response to SDF-1 defines the leading edge and the direction of cell migration.

## Introduction

Cell migration plays a critical role in early embryonic development, organogenesis, organ function, and homeostasis. Aberrant cell migration, on the other hand, contributes to pathology in diseases such as cancer and chronic inflammation. Elucidating the molecular

mechanisms underlying cell motility and guided migration is therefore an important theme in cell and developmental biology with direct bearing on medical disorders (reviewed in Affolter and Weijer [2005]; Brabletz et al. [2005]; Chisholm and Firtel [2004]; Luster et al. [2005]; Van Haastert and Devreotes [2004]; Vicente-Manzanares et al. [2005], and Yamaguchi et al. [2005]).

In many organisms, primordial germ cells (PGCs) migrate a considerable distance because they are specified at positions distinct from the location of the gonad, where they differentiate into sperm or eggs. PGC migration toward their target thus serves as a valuable *in vivo* model for directed cell migration (reviewed in Kunwar et al., 2006). The use of various genetic tools and labeling techniques in the translucent zebrafish embryo makes this system especially suitable for studies of diverse dynamic cellular processes at a high resolution (e.g., Beis and Stainier [2006]; Gilmour et al. [2004]; Jin et al. [2005]; Sepich et al. [2005]; Torres-Vazquez et al. [2004], and Ulrich et al. [2005]), including PGC migration (reviewed in Raz [2003] and Raz and Reichman-Fried [2006]).

Following their specification, zebrafish PGCs undergo a series of morphological changes prior to becoming motile cells capable of responding to attractive cues (Blaser et al., 2005). The ensuing migration of PGCs toward their intermediate and final targets is guided by stromal-cell-derived factor-1a, SDF-1a/CXCL12a (Doitsidou et al., 2002; Weidinger et al., 1999, 2002), which acts through its G protein coupled receptor, CXCR4b (Doitsidou et al., 2002; Knaut et al., 2003). PGCs in which the activity of CXCR4b is knocked down are motile but migrate nondirectionally (Doitsidou et al., 2002; Knaut et al., 2003). SDF-1-CXCR4 signaling is also critical for a wide range of cell-migration processes in vertebrates during development, in trafficking of hematopoietic cells in the adult organism, and in pathological conditions resulting from abnormal cell movement (reviewed in Burger and Kipps [2006]; Lapidot et al. [2005]; Murdoch [2000], and Zlotnik [2006]). Despite the central role this pathway plays in these various processes, the molecular and cellular mechanisms that translate SDF-1 signaling into cell polarization and directed migration are largely unknown.

An important mechanism for controlling cell polarization and migration involves increased actin polymerization at the leading edge of migrating cells (reviewed in Pollard and Borisy [2003]; Rafelski and Theriot [2004], and Small and Resch [2005]). An additional mechanism has been proposed suggesting that hydrostatic pressure in the cytoplasm constitutes the driving force for deformations of the cell surface by the generation of protrusions or blebs (Bereiter-Hahn et al., 1981; Bray and White, 1988; Charras et al., 2005; Janson and Taylor, 1993). According to this model, myosin-dependent contractility at the cell cortex generates local hydrostatic pressure (Charras et al., 2005) or ruptures in the cortex (Paluch et al., 2005, 2006; Sheetz et al., 2006) that lead to membrane detachment from the cytoskeleton and flow of cytoplasm that expands the cellular protrusion.

\*Correspondence: eraz@gwdg.de

<sup>5</sup>These authors contributed equally to this work.

<sup>6</sup>Present address: Department of Cell and Developmental Biology, University of Pennsylvania School of Medicine, Philadelphia, Pennsylvania 19104.

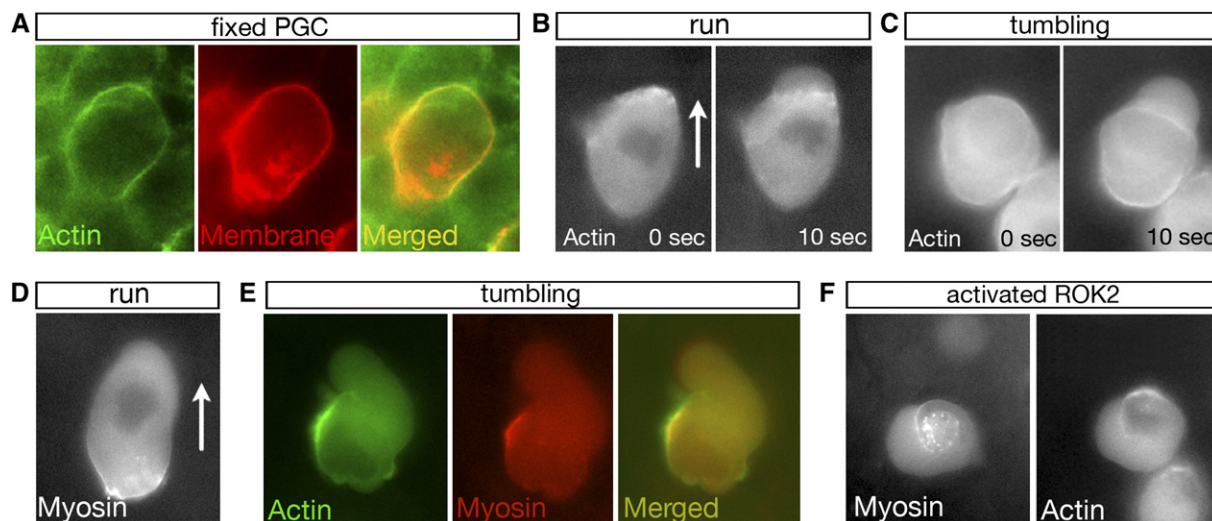


Figure 1. Distribution of Actin and Myosin in PGCs

(A) PGCs in fixed embryos showing an actin belt (phalloidin green) at the cell perimeter along the cell membrane (red). (B–F) Snapshots from time-lapse movies of cells at 10–12 hr postfertilization (hpf). (B) EGFP-actin distribution in migrating PGCs during run or (C) tumbling phases (Movies S1 and S2, respectively). (D) The distribution of EGFP-myosin II heavy-chain fusion protein in migrating PGCs during run phase (Movie S3). (E) Actin (green) and myosin (red) distribution in tumbling cells. (F) EGFP-myosin (left panel) and EGFP-actin (right panel) distribution in PGCs expressing constitutively activated ROK2. Arrows indicate the direction of migration.

It was also shown that acto-myosin contraction could be regulated by an influx of calcium ions into the cell (Strohmeier and Bereiter-Hahn, 1984, 1987), presumably by activating calcium-dependent kinases that mediate myosin contractility (reviewed in Matsumura, 2005). The precise region where a bleb forms could depend on the level of local hydrostatic pressure (Charras et al., 2005) or on the position where contractility generates breaks in the cell cortex (Paluch et al., 2005, 2006; Sheetz et al., 2006), as well as on the local strength of the connection between the membrane and the actin-based cortical cytoskeleton (Sheetz et al., 2006).

In this work, we have studied the mechanisms controlling shape changes and directional motility of germ cells performing chemotaxis in response to the chemo-kine SDF-1a. We show that polymerized actin is not enriched underneath the expanding cell membrane and therefore does not appear to power the generation of cellular protrusions. Instead, protrusion formation depends on acto-myosin contraction. The finding that calcium concentration is elevated at the front of the migrating cells provides a mechanism for increasing local myosin contraction that could contribute to the separation of the plasma membrane from the cytoskeleton and to protrusion formation. In conclusion, we suggest that streaming of cytoplasm in response to pressure generated by acto-myosin contraction constitutes a major force propelling cellular extensions in zebrafish PGCs. Increased calcium level that is controlled by SDF-1a signal could determine the position of protrusion formation, thus defining the leading edge of the migrating cell.

## Results

### Distribution and Dynamics of Cytoskeleton Components in Migrating PGCs

Guided toward their targets by the chemoattractant SDF-1a, migrating zebrafish PGCs persistently alternate

between two modes of behavior; in one, they are polarized and extend protrusions primarily in the direction of their movement (a phase referred to as “run”), and in the other, polarization is lost and the cells remain on the spot as they extend protrusions in all directions (“tumbling” phase) (Reichman-Fried et al., 2004). To define the molecular mechanisms that control PGC morphology, motility, and directed migration we sought to determine the distribution of actin and myosin and thus, their potential contribution to migration of these cells.

The RNA of both actin and myosin is maternally provided and ubiquitously expressed in the developing embryo (Figure S3; see the Supplemental Data available with this article online). To determine the subcellular distribution of actin, we examined PGCs in fixed embryos by staining with the F-actin-binding substance phalloidin and established the presence of polymerized actin at the cortex along the membrane contours of these cells (Figure 1A). Actin localization was then monitored in live PGCs by following the distribution of an EGFP-actin fusion protein in the cells. We have observed asymmetric distribution of actin in polarized PGCs during run phases such that a higher concentration of actin was often detected at the cell front (Figure 1B,  $t = 0$  s). However, invariably, as the cells generate protrusions in the direction of migration, the leading edge of the cell extends beyond the actin belt and, itself, shows no enrichment in actin (Figure 1B,  $t = 10$  s, and Movie S1). When PGCs lose their polarization and enter the tumbling phase, new protrusions that are formed at random sites around the cell perimeter consistently advance past the actin cortex and do not exhibit elevated actin levels (Figure 1C and Movie S2). Both Cortactin-EGFP and 34 kDa-EGFP fusion proteins that bind to F-actin (Furukawa et al., 2003; Kaksonen et al., 2000; Weed et al., 2000) display a similar distribution pattern to that of EGFP-actin relative to forming protrusions (Figure S1). These results indicate that in contrast to several other

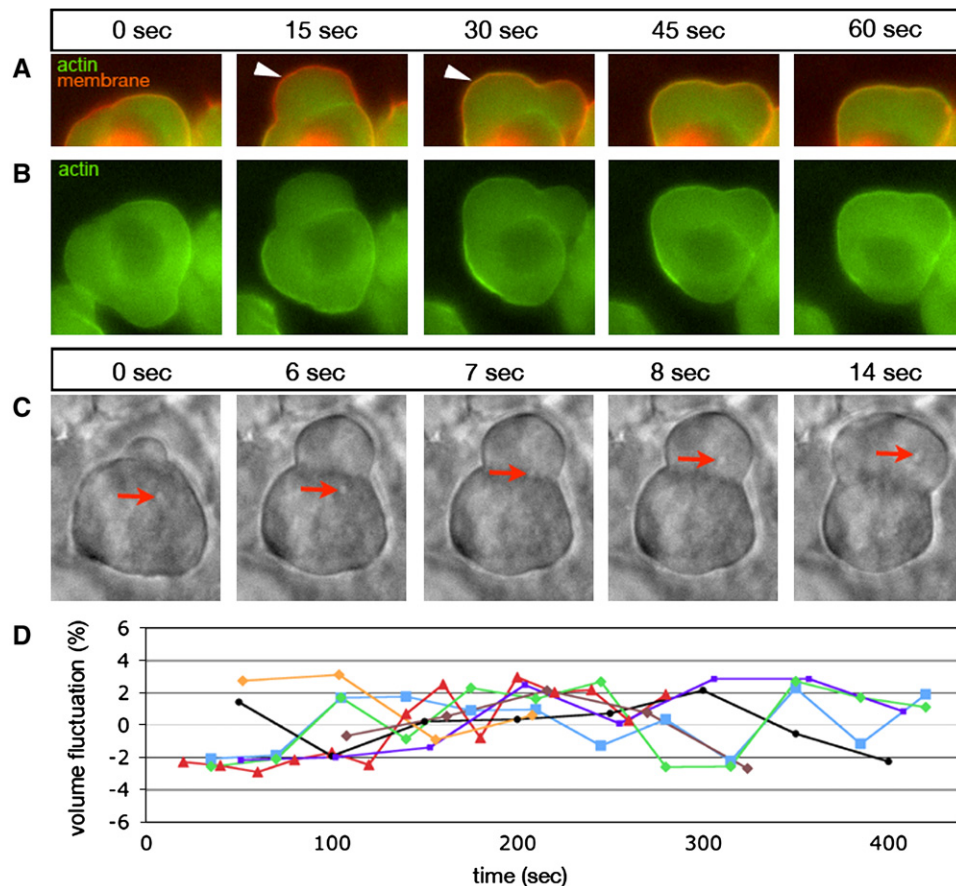


Figure 2. Bleb Formation in PGCs

(A–B) Tumbling PGCs expressing EGFP-actin and farnesylated DsRed labeling the membrane in red, as monitored by time-lapse microscopy. (A) The dynamics of the plasma membrane relative to the actin cortex at the site of a forming protrusion reveals the separation of the plasma membrane (red) from the cortex (green) ( $t = 15$  s, arrowhead) and reassembly of actin at the rim of the retracting protrusion ( $t = 30$  s, arrowhead) (Movie S4). The sequence of these cellular events was validated by similar results obtained when the order of imaging actin (green channel) and membrane (red channel) was reversed (Figure S2). (B) Distribution of EGFP-actin alone in the same cell as in (A). (C) Snapshots showing flow of cytoplasm in which a white particle (red arrow) drifts into an inflating protrusion (Movie S5) while the rear of the cell is stationary. (D) Volume measurements of seven PGCs during run and tumbling phases showing no significant alterations in cell volume during migration.

cell types (Pollard and Borisy, 2003; Rafelski and Theriot, 2004), the driving force for the formation of protrusions in zebrafish PGCs is unlikely to be actin polymerization.

To determine the distribution of myosin in migrating PGCs, we have examined cells expressing myosin II heavy-chain fused to EGFP. During run phases, increased myosin concentration was detected in the back of polarized PGCs, although the fusion protein was also found in other parts of the cell including its front (Figure 1D and Movie S3). In tumbling PGCs, myosin was distributed in a similar manner to that of actin with the two proteins often colocalized at variable regions of the cell periphery (Figure 1E). Thus, along with the role myosin could play in retraction of the rear of migrating cells, cortical and cytoplasmic myosin could generate contractile force at additional sites.

#### Formation of Bleb-like Protrusions in PGCs

To gain insight into the cellular mechanisms responsible for pseudopod formation, we labeled the actin cytoskel-

eton and the cell membrane of tumbling germ cells and closely monitored the generation of cellular extensions. This analysis revealed that a protrusion occurs as the membrane detaches from the actin-containing cortex and that actin is not enriched at the front nor in the interior of the advancing protrusion (Figures 2A and 2B,  $t = 15$  s, and Movie S4). Once protrusion expansion is completed, new cortical actin is assembled underneath the cell membrane, while the cortical actin left behind gradually disassembles (Figure 2B,  $t = 30$ – $60$  s, and Movie S4). Then, as the pseudopod begins to shrink, the newly assembled cortex becomes increasingly prominent at the rim of the retracting protrusion (Figures 2A and 2B,  $t = 60$  s, and Movie S4). It is noteworthy that visualization of myosin relative to the plasma membrane in the course of expansion and retraction of pseudopodia revealed similar dynamics to that of actin (Figure S2A), suggesting cooperation of actin and myosin at the cell cortex. Together, extension of a new pseudopod by migrating PGCs involves separation of the plasma membrane from the actin cortex, possibly at sites of weakened

attachments and outwards progression of the membrane without showing increased level of actin anywhere in the expanding protrusion.

An attractive alternative mechanism to the one implicating actin polymerization as a driving force for membrane inflation is the flow of cytosol through regions of the cortex that are weakly attached to the plasma membrane (Bereiter-Hahn, 2005; Charras et al., 2005; Paluch et al., 2006; Raucher et al., 2000). Indeed, when PGCs were examined by light microscopy, cytoplasmic streaming into the forming protrusion was clearly evident (Figure 2C and Movies S5 and S6). It is therefore conceivable that the vectorial movement of cytoplasm into the expanding pseudopod powers the shape changes of PGCs. Finally, the finding that during migration the volume of germ cells remains virtually constant ( $\pm 3\%$ ) (Figure 2D) is consistent with the idea that the protrusions are produced primarily by cytoplasmic flow rather than as a result of water crossing the plasma membrane.

#### Alterations in Contractility of the Acto-Myosin Network Lead to Abnormal PGC Migration

PGCs normally reach the site at which the gonad develops within the first 24 hr of embryonic development and cluster at a region of high SDF-1a concentration (Figure 3A, right panel) (Doitsidou et al., 2002; Weidinger et al., 1999; Yoon et al., 1997). Migration toward the target involves protrusive activity primarily at the leading edge of migrating germ cells (Figure 3A and Movie S7), whereas tumbling cells, or cells that have reached their target, extend protrusions randomly around the cell perimeter (Reichman-Fried et al., 2004). As presented above, this activity is accompanied by dynamic changes in the cell cortex and appears to be driven by cytoplasmic flow into the inflating protrusion.

Contraction of the acto-myosin network has been suggested to generate internal hydrostatic pressure, which could push the cytosol into the forming pseudopod (Bereiter-Hahn et al., 1981; Bray and White, 1988; Charras et al., 2005; Janson and Taylor, 1993). To investigate whether this model applies to the formation of cellular protrusions in migrating PGCs, we have manipulated the activity of myosin II and determined the effect on cell morphology and directed migration. It is expected that inhibition of myosin activity should diminish cortex contractility. This would reduce local hydrostatic pressure or formation of ruptures in the cortex and consequently inhibit protrusive activity. Conversely, a global enhancement of myosin activity should induce stronger and more persistent cortical contractions and hence promote the formation of larger and longer-lived blebs in random directions. To carry out such manipulations, we took advantage of the fact that the phosphorylation state of the regulatory light chain of myosin II (MLC) is the primary determinant controlling myosin-II activity (Matsumura, 2005; Moussavi et al., 1993).

An important regulator of MLC activity is Rho kinase (ROK/ROCK). ROK can activate myosin II contractility directly by phosphorylating MLC and, indirectly, by phosphorylating and thereby inhibiting the function of the MLC phosphatase (Matsumura, 2005). Furthermore, the calcium-dependent MLC kinase (MLCK) and the death-associated protein kinase (DAPK) activate MLC

and appear to play a role in cell polarity during migration and tumor-cell invasion (Kuo et al., 2006; Shohat et al., 2002). Consistent with the notion that these kinases regulate myosin function in zebrafish PGCs, the RNAs encoding for ROK2, MLCK, and DAPK are ubiquitously and uniformly expressed in zebrafish embryos at the four- to eight-cell stage (maternally provided transcripts) and at the two- to four-somite stages (Marlow et al., 2002) (Figure S3). To determine whether altering myosin activity levels would affect migration behavior of zebrafish PGCs, we expressed constitutively active and dominant-negative forms of ROK2, MLCK, and DAPK in these cells. Whereas no effect on somatic development could be detected (Figures 3B, 3C, 3E, and 3F, right panels), manipulating the activity of these kinases in PGCs interfered with cell migration; unlike cells in control embryos, which by 24 hr postfertilization (hpf) were clustered at the site of the prospective gonad, a considerable number of cells in experimental embryos were found in ectopic positions (40%–80% of germ cells were ectopic in 14–50 embryos examined in each experiment) (Figures 3A–3C, 3E, and 3F, right panels). To determine the basis for the migration phenotypes, we examined the morphology of the manipulated cells at a higher resolution. We found that in PGCs expressing constitutively active ROK2, actin and myosin were localized toward the center of the cell, clearly separated from the plasma membrane (Figure 1F). The separation between the membrane and the cortex allows the cells to repeatedly extended broad protrusions that once generated, continued to advance around the cell perimeter (Figure 3B and Movie S8). Significantly, elongated long-lived protrusions that advanced around the cell perimeter were observed in migrating PGCs expressing constitutively active versions of the calcium-dependent kinases MLCK or DAPK (Figure 3E, Movie S11, and data not shown). The morphological difference between the protrusions induced by these kinases could stem from the distinct modes of MLC activation, the level of activation, as well as from differences in the subcellular localization of the proteins (Matsumura, 2005; Totsukawa et al., 2004). In accordance with these results, the ability of cells exhibiting aberrant protrusions of this kind to migrate directionally is impaired, as observed in the tracks delineating their route of migration; while tracks representing migration routes of control PGCs are stretched out, those of experimental cells are more coiled and less directional (tracks in Figures 3B and 3E). It is interesting to note that formation of similar long protrusions around the cell perimeter was observed in PGCs that were subjected to very high levels of the guidance cue SDF-1a (Doitsidou et al., 2002), consistent with the idea that CXCR4b activation is translated into enhanced myosin contractility. A different effect on PGC morphology and migration was induced in cells expressing the dominant-negative form of ROK2 (DN-ROK2). In this case, affected cells cease to extend pseudopodia, assumed a round cell shape, and barely moved (Figure 3C and Movie S9). Similarly, coexpression of dominant-negative forms of the two calcium-dependent kinases DAPK (DN-DAPK) and MLCK (DN-MLCK) often led to a strong reduction in pseudopod formation, while filopodia production, which solely depends on elongation of actin filaments (Mejillano et al., 2004), was not affected

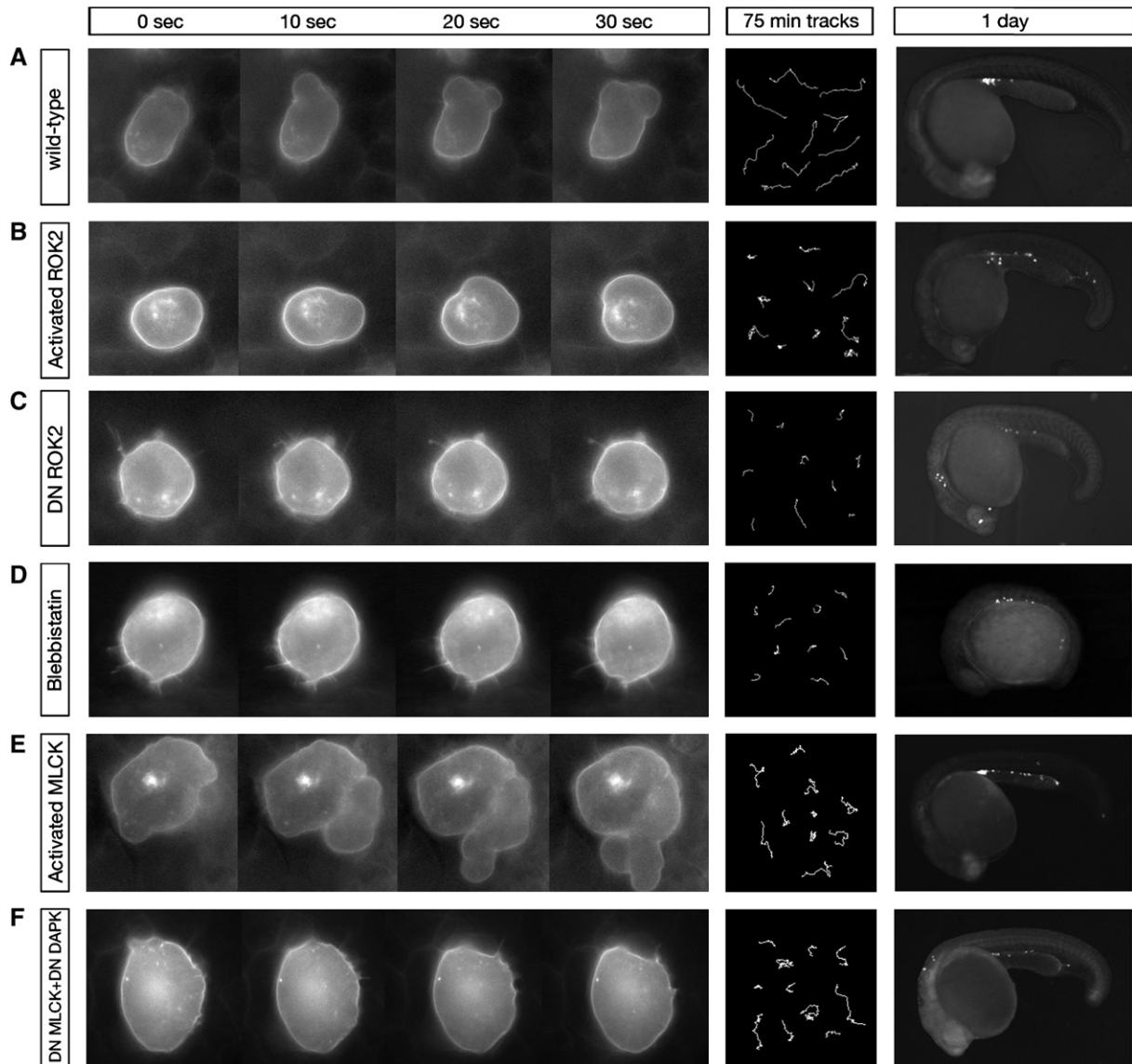


Figure 3. Alterations of Myosin Contractility in PGCs Lead to Abnormal Cell Morphology and Defective Migration

(A–F) Panels from left; snapshots from time-lapse movies showing cell morphology of PGCs whose membrane is labeled with EGFP. The track panels delineate routes along which PGCs migrated in the embryos for 75 min (for each experiment, ten PGCs from two to three embryos were sampled), and the right panels show the position of EGFP-labeled PGCs in 1 day old embryos. (A) Wild-type PGCs exhibit polarized cell shape as they actively migrate (Movie S7) along mostly linear routes while advancing toward their final target. (B) PGCs expressing constitutively activated ROK2 form broad protrusions that extends around the cell perimeter (Movie S8). Many of the migration tracks are nondirectional and coiled. One-day embryos show PGCs at abnormal positions. (C) PGCs expressing dominant-negative ROK2 (Movie S9) show a round cell shape. Short tracks reflect inhibition of migration and are the basis for the inability of most cells to reach their target at 1 day. (D) PGCs from embryos treated with blebbistatin are round and do not move (Movie S10), as manifested in the short tracks and a severe migration phenotype observed in 1 day old embryos. The development of the drug-treated embryo is delayed. (E) PGCs expressing constitutively active MLCK display large and complex protrusions that extend around the cell perimeter (Movie S11). The tracks span short distances, and many cells do not reach the final target. (F) PGCs coexpressing dominant-negative MLCK and dominant-negative DAPK show minimal protrusive activity and simple cell shape (Movie S12). The tracks are short, and the embryos exhibit numerous ectopic PGCs.

(Figure 3F and Movie S12). It appears, therefore, that pseudopod formation in PGCs is strongly dependent on myosin activation by phosphorylation. Consistently, in embryos treated with the myosin II inhibitor, blebbistatin (Kovacs et al., 2004; Straight et al., 2003), the PGCs continued to extend filopodia but lost their ability to form pseudopods and consequently rounded up and stopped migrating (Figure 3D and Movie S10).

#### Myosin Is Activated at the Front of Migrating PGCs

Considering that MLC phosphorylation is at the basis of myosin function in exerting contractile forces, we wished to determine the spatial and temporal distribution of its kinase, MLCK, in migrating PGCs. We found that MLCK was localized primarily to the front of polarized migrating germ cells and, to a lesser extent, to the back or the sides of the cells (Figure 4A). Moreover,

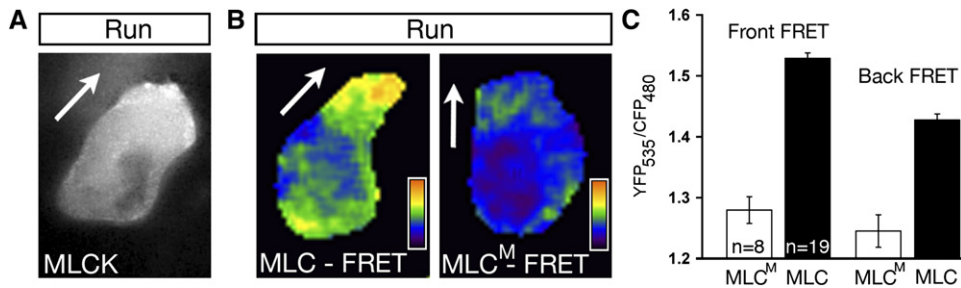


**Figure 4. Localization of MLCK and Phosphorylated Myosin Light Chain in PGCs**  
 (A) PGCs during run phase show localization of MLCK-GFP fusion protein to the cell front (n = 4 cells).  
 (B) Distribution of FRET signal in polarized PGCs expressing wild-type myosin light chain (MLC) protein in a FRET construct (MLC-FRET, left panel). The intensity of the FRET signal indicates the level of phosphorylated MLC and, thus, of myosin activation. Pseudocolor bars represent the range of MLC phosphorylation (blue, low; orange, high). The right panel shows the signal produced by a FRET reporter containing a mutated MLC protein that cannot be phosphorylated (MLC<sup>M</sup>-FRET).  
 (C) A graph representing YFP<sub>535</sub>/CFP<sub>480</sub> ratio, signifying the FRET signal as measured in the front and back of PGCs expressing either MLC-FRET or MLC<sup>M</sup>-FRET. The values illustrate the lack of myosin activation in cells expressing MLC<sup>M</sup>-FRET. A significant difference in FRET between front and back is measured in PGCs expressing MLC-FRET reporter. Arrows point to the direction of migration. n represents the number of PGCs analyzed, and error bars represent the standard error of the mean (SEM).

the highest activation of MLC, as determined by a fluorescence resonance energy transfer (FRET) signal, was observed in the front of migrating PGCs and a lower, yet detectable, signal was seen in the back (Figure 4B, left panel, and Figure 4C). A control mutated MLC reporter that cannot be activated (MLC<sup>M</sup>, containing mutated phosphorylation sites) showed a weak FRET signal, with no significant difference between the front and the back (Figure 4B, right panel, and Figure 4C). In conclusion, the localization of highly phosphorylated MLC at the front of migrating PGCs is likely to reflect increased myosin-mediated contractility at that site. The low expression of MLCK at the back of polarized germ cells indicates that another kinase might activate MLC in this region (e.g., ROK2 in analogy to ROCK activity in neutrophils) (Xu et al., 2003).

#### Calcium Levels Are Increased in Cellular Protrusions and at the Cell Front of Polarized PGCs

One of the earliest responses to CXCR4 activation by SDF-1 is an increase in intracellular calcium (Bleul et al., 1996; Oberlin et al., 1996), thus raising the possibility that this ion serves as a second messenger relaying the SDF-1 signal. To visualize the distribution of free calcium in PGCs, we have loaded the cells with the calcium-sensitive dye Dextran-conjugated Oregon green BAPTA and recorded the fluorescence intensity by time-lapse confocal microscopy. Interestingly, we found that the level of free intracellular calcium was significantly higher in protrusions as compared with other regions of the cell where no protrusive activity was observed (Figure 5A and Movie S13). Comparing the distribution of Oregon green BAPTA with that of cytoplasmic DsRed and Dextran-conjugated Alexa568 further substantiated this result; whereas DsRed and Alexa568 were evenly distributed in the cell, higher calcium level was consistently observed at the protrusion site (Figure S4 and data not shown). To determine whether this phenomenon depends on SDF-1 signaling, we have measured calcium levels in PGCs knocked down for CXCR4b or SDF-1a activity. Both manipulations resulted in a significant reduction of free calcium in protrusions

as compared with wild-type control PGCs (Figures 5B and 5F, Movie S14, and data not shown). Importantly, during run phases, polarized wild-type PGCs displayed a high calcium level at the cell front, while cells knocked down for CXCR4b showed lower calcium level at the front as they migrated nondirectionally (Figure 5E, Movie S17, and data not shown).

#### Cellular Calcium Is Required for Proper Germ-Cell Migration

To investigate the functional significance of the increased calcium in pseudopods, we interfered with calcium elevation in germ cells by overexpressing calcium-binding proteins that buffer intracellular calcium. Specifically, we used Parvalbumin and CalbindinD28k that act as “calcium buffers” in muscle and neuronal cells (Chard et al., 1993; Pechere et al., 1977). Indeed, expression of membrane-bound zebrafish Parvalbumin (PRV-F) or mouse CalbindinD28k (CLB28-F) in PGCs lowered, although did not completely abolish, the free calcium levels in pseudopods (Figures 5C and 5F and Movie S15). As a control, we overexpressed a calcium-binding-defective mutant form of Parvalbumin at the cell membrane (PRV<sup>m</sup>-F according to Rhyner et al., 1996) that did not alter significantly the calcium levels in protrusions (Figures 5D and 5F and Movie S16). These findings provided useful tools for examining the role of calcium in protrusion formation and directed PGC migration. Notably, PGCs expressing PRV-F migrated abnormally with a significant fraction of cells arriving at ectopic locations after 23 hr of development (an average of 36% ectopic cells in 27 embryos examined) (Figure 6B). This is in contrast to normal migration exhibited by germ cells expressing the control protein, PRV<sup>m</sup>-F (an average of 2% ectopic cells in 28 embryos examined) (Figure 6A). It is noteworthy that in situ hybridization analysis of experimental embryos revealed a normal expression pattern of the guidance cue SDF-1a. Thus, the observed migration phenotype resulted from calcium reduction in PGCs themselves rather than from defects in differentiation of somatic cells along the migratory route (Figures 6A and 6B, left panels).

To determine the cellular basis for the defective migration, we initially measured the overall cell migration speed. PGCs overexpressing PRV-F or CLB28-F exhibited a reduced migration speed relative to control germ cells expressing PRV<sup>m</sup>-F (Figure 6C). Although upon CXCR4 knockdown, the duration of run was significantly reduced, that is, from 13.5 to 8 min, to the extend calcium was experimentally buffered, the speed and the duration of run were not effectively influenced (Figure 6D and data not shown). In contrast, upon calcium buffering, the relative time spent in the tumbling phase was dramatically increased (Figure 6E); the latter can be accounted for by enhanced persistence of tumbling phase (25 min in experimental cells as opposed to 8 min in the control). Therefore, it is possible that the main defect brought about by reducing calcium levels is the failure to repolarize and establish a leading edge to exit the nonpolarized tumbling phase. Last, the reduced efficiency of gonad colonization exhibited by the manipulated cells is probably due to their overall slower migration speed. The fact that the migration targets for PGCs dynamically shift their position during normal embryonic development leads to cases where slowly migrating cells lose their correct target and are attracted to alternative SDF-1a-expressing domains (e.g., Dumstrei et al., 2004).

#### Local Increase in Calcium Levels Promotes Protrusive Activity of PGCs

The findings showing increased calcium levels at the cell front and in forming protrusions along with disruption of PGC migration upon reducing calcium levels prompted us to examine the effect of the reverse manipulation, namely, local elevation of calcium levels. To this end, we used the STIM1 protein that controls calcium influx in response to depletion of internal calcium stores (Liou et al., 2005; Roos et al., 2005; Zhang et al., 2005). Low calcium levels in the endoplasmic reticulum (ER) triggers interaction of STIM1 with calcium channels on the plasma membrane, resulting in increased calcium influx. A specific mutation in the calcium-binding domain of STIM1 (STIM1-D76A or STIM1<sup>M</sup>) leads to a constitutive translocation of the protein close to the plasma membrane, thereby facilitating calcium entry irrespective of the calcium level in the ER (Liou et al., 2005; Roos et al., 2005; Zhang et al., 2005). To determine whether the STIM1 protein is localized to the ER in PGCs as was previously described for other cell types (Liou et al., 2005; Zhang et al., 2005), we followed the distribution of DsRed-STIM1 fusion protein in migrating germ cells. Indeed, wild-type STIM1 protein was primarily localized to the ER and rarely appeared to overlap with the plasma membrane (Figure 7A and Figure S5A, upper panel). On the other hand, depletion of internal calcium stores with the drug thapsigargin, led to a shift of STIM1 fluorescence that overlapped with the membrane signal (Figure S5B). Importantly, a similar protein localization pattern was observed for the mutant form of STIM1 (STIM1<sup>M</sup>) (Figure 7B and Figure S5A).

PGCs expressing STIM1<sup>M</sup> exhibited higher levels of calcium at sites where the mutant STIM1 protein was localized (Figure 7F and Figure S5C) and formed blebs at these locations (Figures 7B and 7C and Movie S18). The correlation between STIM1 localization and formation of

protrusions provides further support for the notion that calcium can locally induce protrusion formation. To determine whether the generation of blebs attributed here to the elevation in calcium depends on myosin contraction, we have inhibited myosin activity while expressing STIM1<sup>M</sup> in the PGCs. Importantly, we observed a dramatic suppression of STIM1<sup>M</sup>-induced protrusive activity in cells expressing a dominant-negative form of ROK2 (Figure 7D and Movie S19) and in cells treated with the myosin II inhibitor, blebbistatin (Figure 7E). Finally, to examine the role of polarized calcium distribution in PGC migration, we have followed cells expressing the mutated STIM1 by time-lapse microscopy. We found that manipulated cells in which calcium levels were elevated at the back showed migration defects manifested in shorter migration tracks and the arrival of PGCs at ectopic positions (Figure 7G). This phenotype is likely to stem from slower migration during run phases as well as from defects in assuming cell polarity as evident by the increased duration of the nonpolar tumbling phases (Figure 7H).

#### Discussion

Current models for animal cell migration are dominated by the view that increased actin polymerization at the cell front coupled with unbending of the filaments against the cell membrane provide the driving force for the protrusion formation in the direction of migration (Chisholm and Firtel, 2004; Pollard and Borisy, 2003; Rafelski and Theriot, 2004; Small and Resch, 2005; Van Haastert and Devreotes, 2004). In these models, the function of myosin-based contraction is centered on retraction of the rear rather than actively participating in pseudopod formation at the leading edge. This description of cell migration applies for important in vitro models for cell motility such as in fish epidermal keratocytes and fibroblasts as well as in directionally migrating cells responding to chemotactic cues such as *Dictyostelium* cells (Bear et al., 2000; Svitkina et al., 1997; Van Haastert and Devreotes, 2004; Verkhovskiy et al., 1995, 1999). In *Dictyostelium*, localization of PtdIns(3,4,5)P<sub>3</sub> (PIP3) to the leading edge of the cell is correlated with enhanced actin polymerization and pseudopod formation. However, *Dictyostelium* cells in which PIP3 production is reduced remain responsive to directional cues (Van Haastert and Devreotes, 2004). Thus, in the absence of polarized PIP3 on the membrane, the cells could employ PIP3-independent underlying mechanism for directional sensing and chemotaxis.

PGC migration in zebrafish provides a unique model for investigating cell polarization and directional migration in vivo at a high resolution, in the context of a live vertebrate organism. An important difference between zebrafish PGCs and *Dictyostelium* cells is that the former exhibit uniform distribution of PIP3 on their membrane (Dumstrei et al., 2004). Considering that depletion of PIP3 in zebrafish PGCs has no effect on their ability to migrate in the correct direction (Dumstrei et al., 2004), it is conceivable that these cells employ a different strategy for chemotaxis, perhaps one that is shared with *Dictyostelium* cells deficient for PIP3.

Our results allow us to propose the following model for the signaling events controlling pseudopod

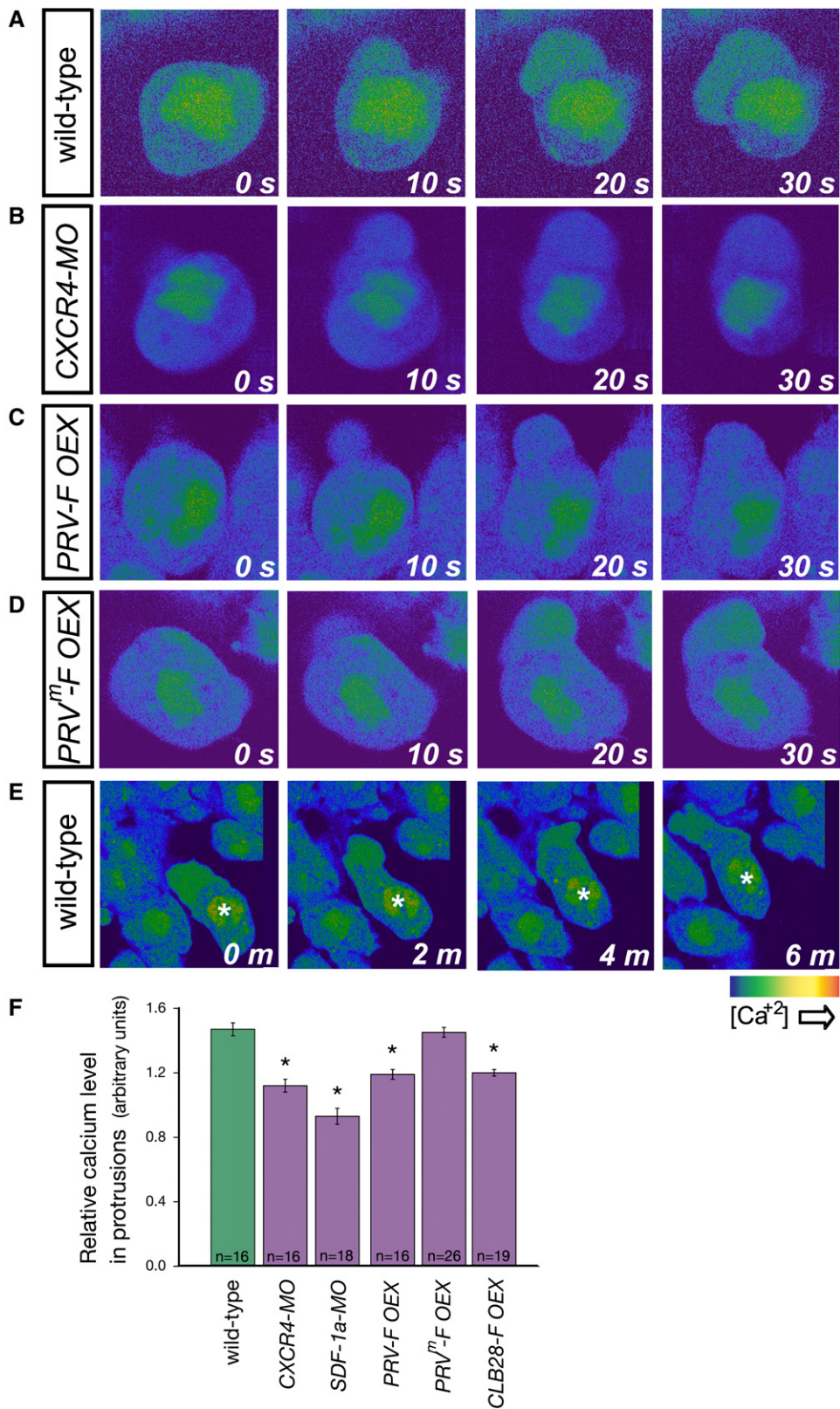


Figure 5. Calcium Levels in Protrusions and at the Front of Migratory PGCs

(A–E) Snapshots from time-lapse movies showing PGCs loaded with the calcium-sensitive dye, Oregon green, as imaged by confocal microscopy. Images are shown in pseudocolors where the bar represents the range of calcium concentrations (low, blue, to high, orange), and s signifies seconds. (A) Wild-type PGCs show high calcium levels in forming protrusions (representing 21 protrusions of 16 PGCs) (Movie S13). (B) PGCs knocked down for CXCR4b by morpholino antisense oligonucleotides show significantly reduced free calcium levels in protrusions (representing 20 protrusions of 17 PGCs) (Movie S14). (C) PGCs expressing a membrane-bound calcium-buffering protein, farnesylated Parvalbumin

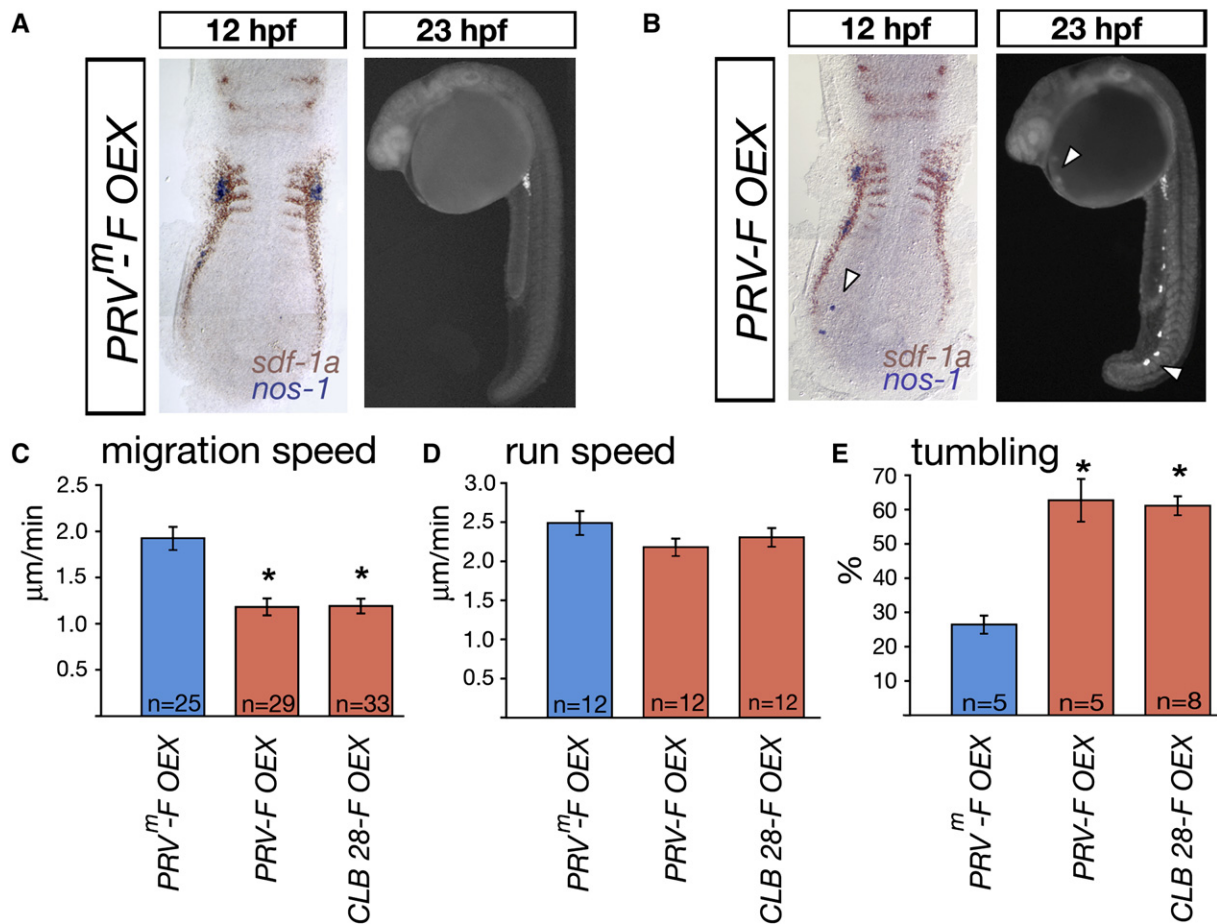


Figure 6. Calcium Buffering in PGCs Leads to Aberrant Migration

(A) PGCs expressing membrane-bound mutated Parvalbumin (PRV<sup>m</sup>-F) arrive at their targets as normal. (B) Expression of membrane-bound wild-type Parvalbumin (PRV-F) in PGCs results in arrival of several PGCs at positions where SDF-1a is not expressed (arrowhead, left panel). At 23 hpf, several PGCs did not reach their final target (arrowheads, right panel). The left panels in (A) and (B) show PGCs stained by in situ hybridization with the germ-cell marker *nos1* (blue) relative to *sdf-1a* expression pattern (brown) in 12 hr embryos. The right panels in (A) and (B) show 23 hr embryos with GFP-labeled PGCs. (C) A graph representing the average speed of PGCs overexpressing a mutated Parvalbumin (PRV<sup>m</sup>-F) relative to those expressing wild-type Parvalbumin (PRV-F) or CalbindinD28k (CLB28-F). (D) The average speed of PGCs during run phase. (E) A graph showing the proportion of time experimental PGCs spend in the tumbling phase. The values are presented as a percentage of total migration time (75 min). n indicates the number of cells analyzed, asterisks indicate  $p < 0.001$ , and error bars represent SEM.

formation that facilitate directional cell migration in response to chemotactic cues encoded by SDF-1a (Figure 8). The association between increased calcium levels and generation of pseudopods at these positions suggests that calcium plays a role in the formation or stabilization of such cellular protrusions. In response to calcium elevation, myosin phosphorylation and activation (Matsumura, 2005) could control protrusion formation as observed upon expression of deregulated forms of the calcium-dependent MLCK and DAPK in PGCs. Specifically, while elevated myosin activation

led to an increase in protrusive activity (Figure 3E), inhibition of myosin contraction suppressed protrusion formation (Figure 3F). Thus, calcium-dependent myosin activation could trigger and maintain blebs at the leading edge as evident by the concentration of MLC activation at this site (Figure 4B). Consistently, localization of mutated STIM1 that induces calcium influx at the back of the cell (Figure 7F and Figure S5C) leads to bleb formation at this site (Figure 7C) in a process that relies on myosin contraction (Figures 7D and 7E). At the same time, although we were not able to completely

(PRV-F), display decreased calcium levels in protrusions (representing 55 protrusions of 16 PGCs) (Movie S15). (D) PGCs expressing the membrane-bound mutated Parvalbumin (PRV<sup>m</sup>-F) whose calcium-binding domains are nonfunctional show no effect on calcium levels (representing 45 protrusions of 25 PGCs) (Movie S16). (E) Wild-type polarized PGCs display higher calcium concentration at the cell front during directional migration. A single PGC is marked with an asterisk (m signifies minutes, n = 14 PGCs observed) (Movie S17). (F) A graph showing relative calcium levels in protrusions (calculated as described in Experimental Procedures) in wild-type cells, cells knocked down for SDF-1a or CXCR4b as well as in PGCs overexpressing different versions of calcium-binding proteins. Asterisks indicate  $p < 0.001$ , and error bars represent SEM.

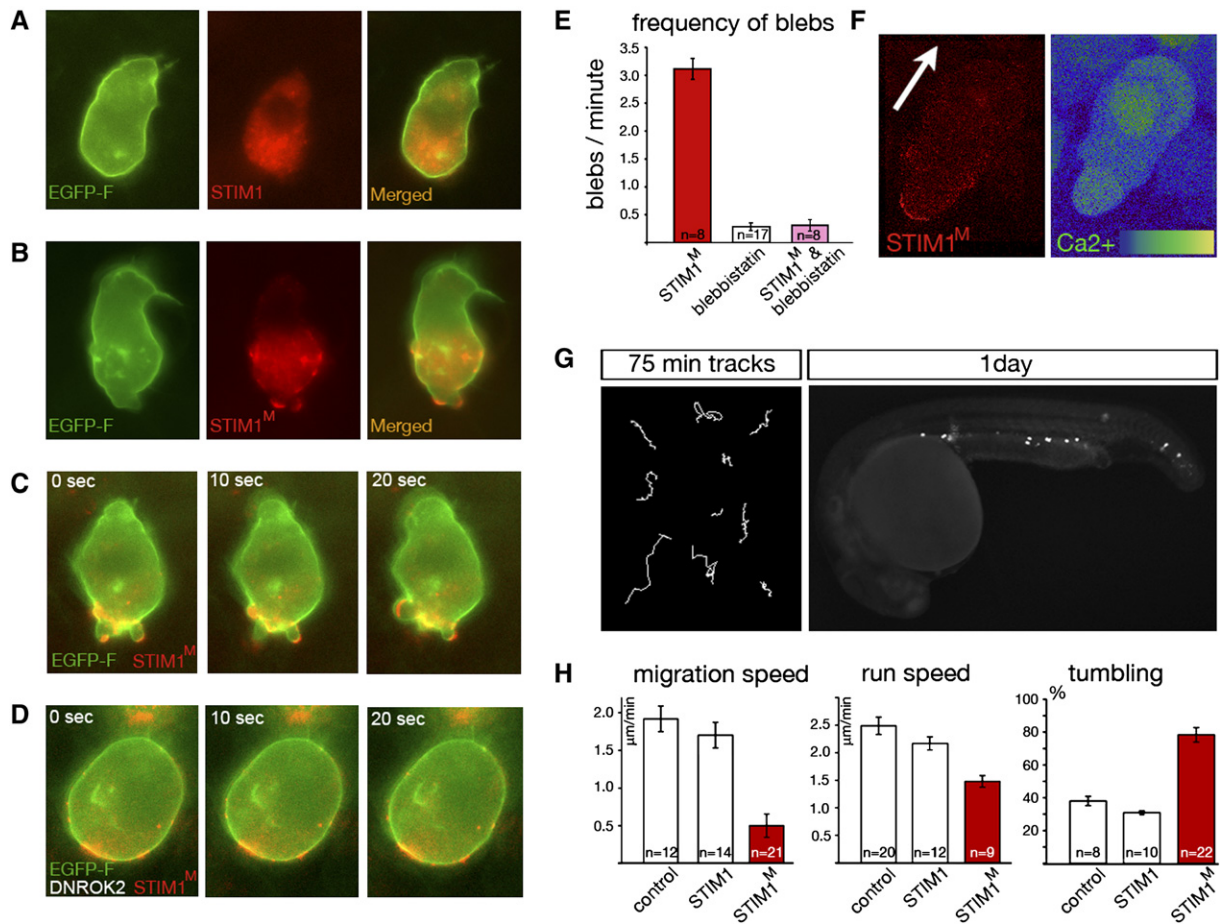


Figure 7. Local Increase in Cellular Calcium Levels Results in Enhanced Myosin-Dependent Protrusive Activity

(A) The wild-type STIM1 protein (red) is found in the cytoplasm.  
 (B) STIM1<sup>M</sup> (red) is localized to the back of the cell and is enriched in puncta close to the plasma membrane (green).  
 (C) Snapshots from a time-lapse movie showing a PGC expressing STIM1<sup>M</sup> (red). The cell shows extensive blebbing primarily at sites of STIM1<sup>M</sup> localization (Movie S18).  
 (D and E) Formation of STIM1<sup>M</sup>-induced blebs depends on myosin function. Expression of a dominant-negative form of ROK2 (D) (Movie S19) or blebbistatin treatment (E) suppress the formation of STIM1<sup>M</sup>-induced blebs.  
 (F) Confocal images of a cell expressing STIM1<sup>M</sup> (left panel, red) showing increased calcium levels at the back of the cell (right panel, pseudo-colors; blue, low; yellow, high).  
 (G) Seventy-five-minute tracks of PGCs expressing STIM1<sup>M</sup> (left panel). PGCs that express STIM1<sup>M</sup> arrive at ectopic positions (n = 27, 1 day old embryos examined, right panel).  
 (H) A graph representing the average total speed (left graph), speed during run (middle graph), and the proportion of time spent in tumbling (right graph) of control PGCs compared with cells expressing STIM1 and STIM1<sup>M</sup>. The values in the right graph are presented as a percentage of total migration time (75 min). n represents the number of cells analyzed, and error bars represent SEM.

buffer calcium levels in the protrusions, a reduction in calcium level clearly delays cell polarization as reflected in the marked increase in the duration of tumbling phases.

Although reduced in magnitude, an increase in calcium in protrusions is also observed in the absence of CXCR4b signaling. It is therefore possible that nondirectionally migrating cells utilize the same cellular mechanism as do SDF-1a-guided cells. The role of SDF-1a then is to dictate the course of migration by determining the site at which the leading edge is established, thereby biasing the direction of CXCR4b-independent cell motility.

Two mechanisms acting each on its own or in combination could translate myosin contraction to pseudopod formation. Acto-myosin contraction could lead to break-

age of the cortical network and local detachment of the membrane from the cytoskeleton followed by inflation of a bleb in response to global hydrostatic pressure (Paluch et al., 2006; Sheetz et al., 2006). Alternatively, local nucleation of membrane detachment could be the consequence of an increase in local hydrostatic pressure generated by the contraction of myosin (Charras et al., 2005). In both cases, the protrusion would be powered by flow of cytoplasm through a region of weakened membrane-cortex attachment into the forming protrusion rather than by increased actin polymerization at the leading edge.

While locally elevated calcium appears to play an instructive role in establishing the cell front, additional factors could cooperate in regulating protrusion formation. For example, phosphatidylinositol 4,5-bisphosphate

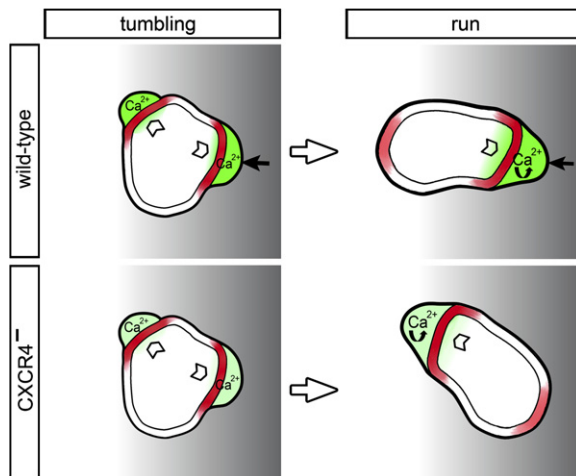


**Figure 8. PGC Polarization in Response to Chemokine Signaling**  
During the apolar tumbling phase, stochastic local increase in calcium (green) at various positions at the cell periphery induces contraction (red) of myosin associated with the actin cortex and leads to separation of the membrane from the cell cortex at weakened attachment sites. Cytoplasmic flow (chevron shapes) into locations of membrane detachment propels the inflation of the protrusion. The gradient of SDF-1 (gray) is responsible for enhanced signaling on one side of the cell (black arrows), thereby amplifying calcium influx that stabilizes a specific protrusion that becomes the leading edge. Consistently, in the absence of CXCR4 signaling and when calcium is buffered, the duration of tumbling phases are increased (this work and data not shown) (Reichman-Fried et al., 2004). During run phases, higher calcium levels are maintained at the front for extended periods as a result of a positive feedback enhanced by receptor activation (in wild-type cells) or as a result of a positive feedback alone (in the absence of CXCR4 signal). Consistently, in the absence of receptor signaling, the duration of run phases is significantly decreased.

(PIP2) has been shown to increase the adhesion energy between the plasma membrane and the cytoskeleton, thereby controlling cell shape (Raucher et al., 2000). An attractive model is that CXCR4-controlled degradation of PIP2 (e.g., by activation of phospholipase C [PLC] generating inositol 1,4,5 trisphosphate [IP3] and diacylglycerol [DAG]), which could account for the relatively high calcium level at the cell front, would also promote protrusion formation by generating spots of reduced adhesion between the membrane and the cytoskeleton. Lowering adhesion strength could involve regulation exerted through proteins linking actin cytoskeleton to the plasma membrane such as the PIP2-binding anchor protein, ezrin (Barret et al., 2000; Tsukita and Yonemura, 1999).

Our observations echo findings of others who have described protrusion formation in migrating cells in vitro that appears to be driven by cytoplasmic flow rather than by actin polymerization. For example, *Dictyostelium* cells exposed to high uniform concentration of cyclic AMP were shown to form blebs by cytoplasmic flow in a process that requires myosin II function (Langridge and Kay, 2006). Similarly, hydrostatic pressure is thought to drive protrusion formation in *Amoeba proteus* (Yanai et al., 1996). Significantly, contractility in the amoeba could be induced by calcium, and in actively migrating cells, calcium was found in the tail as well as at

the leading edge, where pulses of high concentration were observed (Taylor et al., 1980a, 1980b). Similar results have been reported for cancer cells of higher organisms; tumor cells that undergo a transition into an amoeboid mode of migration in three-dimensional (3D) collagen matrix show reduced accumulation of F-actin at the cell front (Wolf et al., 2003). Interestingly, in the same in vitro model system, migration of the tumor cells requires myosin II function (Betapudi et al., 2006). Specifically, myosin IIA and IIB were found in the leading edge, along with the activated form of MLC and pharmacological inhibition of myosin II and of MLCK-impaired migration of these cells (Betapudi et al., 2006). Last, a bleb-associated mode of motility was described for metastatic cell lines migrating through 3D matrix (Sahai and Marshall, 2003). This movement was shown to depend on Rock and ezrin function and to be distinct from cell motility of other tumor cell lines that extended elongated, F-actin-rich protrusions in a Rac-dependent manner (Sahai and Marshall, 2003).

Whereas in this work we focused on zebrafish PGCs, calcium increase is a common response in migrating cells guided by SDF-1, as well as by other guidance cues (e.g., Belmadani et al. [2005]; Bleul et al. [1996]; Henley and Poo [2004], and Oberlin et al. [1996]). It would thus be interesting to determine whether the biochemical and cellular pathways proposed to operate in the PGCs serve as the underlying mechanism of migration for a broader spectrum of cell types.

While some cell types rely primarily on actin polymerization for pseudopod production, others exhibit, in addition, myosin-II-dependent formation of pseudopods (Langridge and Kay, 2006; Wolf et al., 2003; Yanai et al., 1996). It is conceivable, therefore, that both mechanisms cooperate during the migration process in various cell types. As an ultimate case of myosin-dependent pseudopod formation, zebrafish PGC migration represents an excellent model for studying this mode of protrusion generation.

#### Experimental Procedures

##### Zebrafish Strain and Fish Maintenance

Zebrafish (*Danio rerio*) of the AB genetic background were maintained, raised, and staged as previously described (Kimmel et al., 1995; Westerfield, 1995). The Tol-kop-EGFP-F-nos1-3'UTR transgenic fish line was created with the kop-EGFP-F-nos1-3'UTR (Blaser et al., 2005) cloned into the pTol2000 vector (Tol2 transposase vector) (Kawakami et al., 2004). The purified plasmid DNA was coinjected with sense RNA encoding the Tol2 transposase into one-cell-stage fish embryos. The transgene directs EGFP expression to the plasma membrane of PGCs.

##### Whole-Mount In Situ Hybridization and Phalloidin Staining

One- and two-color whole-mount in situ hybridization protocols were performed as described previously (Jowett and Lettice, 1994) with modifications according to Hauptmann and Gerster (1994) and Weidinger et al. (2002). The following digoxigenin-labeled probes were used for in situ hybridization:  $\beta$ -actin, myosin II regulatory light chain (*mrlc*), *mlck*, *dapk*, *sdf-1a* (Doitsidou et al., 2002), *rok2* (Marlow et al., 2002), and *nanos1* (Köprunner et al., 2001). Primers used to amplify these probes by PCR are described in the Supplemental Experimental Procedures. To examine actin and myosin localization relative to the plasma membrane in fixed PGCs, embryos at one-cell stage were microinjected with RNA (300 pg) encoding farnesylated-dsRed monomer (Clontech) fused to the 3'UTR of the *nanos1* gene (Köprunner et al., 2001). Injected embryos were

fixed at four- to six-somite stage and stained with 66 nM of Alexa Fluor 488-phalloidin (Invitrogen).

### RNA Expression Constructs

Capped sense RNA was synthesized with the MessageMachine kit (Ambion) and microinjected into one-cell stage embryos. To direct protein expression to the PGCs, the corresponding open reading frames (ORFs) were fused upstream to the 3'UTR of the *nanos1* (*nos1*-3'UTR) gene, facilitating translation and stabilization of the RNA in these cells (Köprunner et al., 2001). To fluorescently label PGCs, *gfp-nos1*-3'UTR RNA was injected (210 pg per embryo) (Köprunner et al., 2001). To label the membrane of PGCs, *egfp-f-nos1*-3'UTR RNA (Weidinger et al., 2002) or *DsRedex1-f-nos1*-3'UTR RNA was injected (210 pg and 300 pg, respectively).

For visualization of cytoskeleton components in migrating PGCs, the following constructs were used: for actin visualization, 300 pg RNA of *egfp-human  $\beta$  actin* (Clontech) fused to *nos1*-3'UTR was injected. In addition, *cortactin-egfp* (Kaksonen et al., 2000) and 34 *kDa-egfp* (Furukawa et al., 2003) were each fused to *nos1*-3'UTR. RNA was injected at 240 pg and 300 pg, respectively. For myosin visualization, the ORF of the *nonmuscle myosin heavy chain (NMHC) II-A* was amplified from zebrafish cDNA with forward primer ATGT CAGACGCAGAGAAGT and reverse primer TCGACTCACTCTGGT TTGGGTTTC. Three hundred picograms of *egfp-NMHC II-A-nos1*-3'UTR RNA were injected. To label myosin in red, we fused *NMHC II-A* to mCherry (Shaner et al., 2004), and 350 pg of *mCherry-NMHC II-nos1*-3'UTR RNA were injected. To interfere with intrinsic levels of myosin light-chain activation in migrating PGCs and thereby altering myosin contractility, the following constructs were used: the constitutively active and the dominant-negative forms of the zebrafish *ROK2* gene (Marlow et al., 2002) were included in the *N'-ROK2-nos1*-3'UTR and the *C'-ROK2-nos1*-3'UTR constructs, of which 40 pg and 350 pg RNA were injected, respectively. The full-length ORF of mouse *MLCK* was obtained from the EST clone IRAK961J15112Q2 (RZPD). Constitutively active (CA) *MLCK* and dominant-negative (DN) forms were generated according to Wadgaonkar et al. (2003). Specifically, CA-*MLCK* was generated by cloning amino acids 1–1775, thus excluding both the autoinhibitory domain and the calmodulin-binding site (900 pg of *CA-mlck-nos1*-3'UTR RNA were injected). The DN-*MLCK* lacked amino acids 1611–1637, thereby eliminating the kinase activity of the protein. DN-*mlck-nos1*-3'UTR RNA was injected (1200 pg) along with DN-*dapk-nos1*-3'UTR RNA (450 pg). The latter contains the dominant-negative form of the mouse *dapk* gene (S308D in Shohat et al., 2002).

To determine the subcellular localization of *MLCK* in migrating PGCs, the *mlck-fip-nos1*-3'UTR construct was used (300 pg RNA injected). Although *mlck-fip* was initially designed as a FRET-reporter (Chew et al., 2002), for our purpose, we took advantage of the murine *MLCK*<sub>125</sub>-GFP fusion included in the construct.

To buffer calcium in PGCs, we made use of the zebrafish *parvalbumin (prv)* gene, as well as of the mouse *calbindinD28k (clb28)*. The wild-type *parvalbumin* construct includes the ORF of zebrafish *parvalbumin-1* fused to the farnesylation signal sequence. Zebrafish *parvalbumin* was amplified by PCR from cDNA by using the primers GGGATCCATGGCATTGCTGGTATTTC (forward) and GGAATCTTGATGCCTTGACCAAAGAGG (reverse). RNA was transcribed from pSP64-*prv-f-nos1*-3'UTR construct and injected at 900 pg. As a control, a mutated *parvalbumin, prv<sup>m</sup>*, containing nonfunctional Ca<sup>2+</sup>-binding domains, was generated according to Rhyner et al. (1996). The following primers were used for site-directed mutagenesis of the EF hands (D52A, E63V, D91A, E102V): forward, CATTGCCAGG ACAAGAGCGGCTTCATTGAGGAGGATGIGCTTAAAC and reverse, CTGGAGCCTCTGATGGTGACGGCAAGATTGGAGTTGATGIGTTCCG (sites of base substitution are underlined). RNA transcribed from pSP64-*prv<sup>m</sup>-f-nos1*-3'UTR construct was injected at 900 pg. The ORF of the mouse *calbindinD28k* was obtained from adult mouse cerebellum cDNA (RIKEN full-length enriched library, clone 1500015B14) by PCR amplification with the forward and reverse primers GGGATCCGATGGCAGATCCACCTG and GGACTAGTC TCGTTGTCTCCAGCAGAAAG, respectively. *calbindinD28k* was inserted upstream of a farnesylation signal, and RNA transcribed from the construct pSP64-*clb28-f-nos1*-3'UTR was injected at 900 pg.

The wild-type mouse *STIM1* (Liou et al., 2005; Zhang et al., 2005) served to visualize the subcellular localization of the protein in

PGCs. *stim1* was fused to *DsRed* to give the construct pSP64-*DsRedex1-stim1-nos1*-3'UTR (300 pg RNA were injected). To induce calcium influx in PGCs, the RNA encoding a mutated mouse *STIM1<sup>M</sup>* (*STIM1-D76A/D77A*) (Liou et al., 2005; Zhang et al., 2005) fused to *DsRedex1* was injected (300 pg of *DsRedex1-stim1<sup>M</sup>-nos1*-3'UTR RNA). To label the endoplasmic reticulum (ER) of PGCs, we utilized a construct (pSP64-*eyfp-ER-nos1*-3'UTR, 240 pg RNA were injected) that encodes EYFP flanked by the ER-targeting sequence of calreticulin at the N terminus and ER retrieval sequence KDEL at the C terminus (pEYFP-ER, Clontech).

### Morpholino Knockdown Experiments and Application of Drugs

Knockdown experiments with *cxcr4b* and *sdf-1a* morpholino antisense oligo nucleotide injection (0.4 pmol, GeneTools) were performed as previously described (Doitsidou et al., 2002). Blebbistatin (65  $\mu$ M, Calbiochem) was applied to 6 hpf embryos, and PGC migration was recorded after 7 hr incubation. To examine the PGC migration phenotype at 24 hpf, 8 hpf embryos were incubated with 100  $\mu$ M blebbistatin and imaged at the end of the first day of development. To test whether mouse *STIM1* is functional in zebrafish PGCs, *DsRedex1-stim1-nos1*-3'UTR RNA and *egfp-f-nos1*-3'UTR RNAs were coinjected into one-cell stage embryos. Injected embryos were incubated for 6 hr at 28°C and then submerged in 4  $\mu$ M thapsigargin solution (Calbiochem) for 2 hr. Imaging of PGCs was carried out, while treated embryos remained in the thapsigargin solution.

### FRET Measurements with MLC Phosphorylation Biosensor

To detect spatial and temporal activity of the myosin light chain in migrating PGCs, a FRET construct containing a phosphorylation biosensor was used (Yamada et al., 2005). This biosensor includes the *CRCit* cassette in which MLC phosphorylation is detected by measuring FRET between ECFP and citrine fused to the N and C termini of MLC, respectively. Upon MLC activation by phosphorylation, an increase in the FRET signal is detected as an elevation in citrine emission relative to that of ECFP. To measure MLC-FRET (Figure 4B), we used *CRCit-nos1*-3'UTR RNA in which *CRCit* was inserted upstream of *nos1*-3'UTR. *MLC<sup>M</sup>-FRET* refers to *mCRCitAA-nos1*-3'UTR RNA, which contains the mutated form of *CRCit* that cannot be phosphorylated by MLC kinases. Four hundred fifty picograms of each RNA sample were injected. To measure FRET, the donor (ECFP) was excited at 430 nm, and two emission images were captured sequentially at 480 nm and 535 nm. To determine the phosphorylation level of MLC, fluorescence intensity (F)-ratio images of  $F_{535}/F_{480}$  were generated with the ImageJ software (Figure 4B). This ratio was used to represent FRET efficiency. To compare levels of MLC activation within the cell, mean ratio values in selected areas in the front and back of migrating germ cells were calculated.

### Measurement of Calcium Levels

To visualize free calcium in PGCs, embryos were injected with the calcium indicator Oregon green 488 BAPTA-1 (500  $\mu$ M, dextran, 10,000 MW, Molecular Probes O-6798). To reliably identify germ cells, embryos were coinjected with *vasa-DsRedex1-nos1* RNA (180 pg). At 9–12 hpf, migrating PGCs were imaged by confocal microscopy. To determine the calcium levels in specific regions of PGCs, the recorded frames were analyzed as follows: a region of interest, ROI, in the cell was selected, and the fluorescence intensity (F) was calculated with the Quantity-Mode (Stack profile/Statistics) of the Leica TCS SL confocal software provided by Leica. The ratio  $F_{ROI}/F_{nucleus/2}$  was then derived. The signal intensity of the nucleus was chosen as an internal standard, allowing the comparison among different experiments and developmental stages.

### Fluorescence Microscopy and Cell Volume Measurement

Images were obtained with the Axioplan2 microscope (Zeiss) controlled by Metamorph software (Universal Imaging). Time-lapse movies were generated with a 63 $\times$  or 40 $\times$  objective for imaging cell morphology and behavior and a 10 $\times$  objective for speed and track analysis. For speed measurements and tracking of migrating germ cells, the "Track Objects" software module of Metamorph was used. Frames were captured at 0.5, 2, 5, or 10 s intervals for high-magnification movies and at 1 min intervals for the low-magnification movies, with the RT<sub>SE</sub> camera (Diagnostic Instruments, Inc.). To examine actin dynamics relative to the plasma membrane,

EGFP-tagged actin and DsRed-labeled membrane were sequentially imaged with 400 and 200 msec exposure time for each fluorescent channel, respectively. To validate the results presented in Figure 2A, the order of imaging was reversed such that DsRed-labeled membrane was first to be recorded (results presented in Figure S2B). Confocal images were acquired by using the Leica TCS SL microscope. Frames were captured at 0.8 or 6 s intervals for high-magnification movies. Time-lapse movies of PGCs containing the calcium-sensitive dye Oregon green were generated with 488 nm excitation wavelength. Time-lapse movies of PGCs containing the Oregon green and DsRedex1-STIM1<sup>M</sup> were generated with 488 nm and 543 nm excitation wavelength. Cell volume quantification was carried out with embryos at shield stage from Tol-kop-EGFP-F-nos1-3'UTR transgenic line. Transgenic embryos were imaged by a BioRad Radiance 2000 multiphoton confocal microscope. Z stacks of PGCs were obtained continuously, and for each experiment, 25–33 Z stacks were acquired. This was followed by volume rendering of the cells with Volocity software (Improvision, UK). Cell-volume measurements were performed with a modified version of the Cellenger software (C.-P.H., unpublished data). Volume fluctuations were calculated with respect to the mean volume of each cell.

#### Supplemental Data

Supplemental Data include control experiments that further substantiate the subcellular localization of actin, myosin, calcium, and the calcium sensor STIM1 in migrating PGCs. In addition, RNA expression patterns of cytoskeleton components and regulators, movies and technical aspects of experimental procedures are included. These data are available at <http://www.developmentalcell.com/cgi/content/full/11/5/613/DC1/>.

#### Acknowledgments

We thank Rex Chisholm, Steve Farber, Adi Kimchi, Masamitsu Iino, Klemens Rottner, Heikki Rauvala, and Marcus Fechheimer for kindly providing us with DNA constructs and Helen Le-Cordier and Julia Dörries for technical assistance. We are grateful to Elena Kardash for helpful discussions and to Sonia Minina and Ewa Paluch for critical reading of the manuscript. This work was supported by funds from the Max Planck Society and grants from the Deutsche Forschungsgemeinschaft to E.R. and to C.-P.H. H.B. was supported by Roche Research Foundation, I.C. by the Humboldt Foundation, K.D. by a European Molecular Biology Organization long-term fellowship, and L.S.K. by National Institutes of Health grants GM55101 and GM 77770.

Received: June 22, 2006

Revised: September 25, 2006

Accepted: September 29, 2006

Published: November 6, 2006

#### References

Affolter, M., and Weijer, C.J. (2005). Signaling to cytoskeletal dynamics during chemotaxis. *Dev. Cell* 9, 19–34.

Barret, C., Roy, C., Montcourrier, P., Mangeat, P., and Niggli, V. (2000). Mutagenesis of the phosphatidylinositol 4,5-bisphosphate (PIP<sub>2</sub>) binding site in the NH(2)-terminal domain of ezrin correlates with its altered cellular distribution. *J. Cell Biol.* 151, 1067–1080.

Bear, J.E., Loureiro, J.J., Libova, I., Fassler, R., Wehland, J., and Gertler, F.B. (2000). Negative regulation of fibroblast motility by Ena/VASP proteins. *Cell* 101, 717–728.

Beis, D., and Stainier, D.Y. (2006). In vivo cell biology: following the zebrafish trend. *Trends Cell Biol.* 16, 105–112.

Belmadani, A., Tran, P.B., Ren, D., Assimacopoulos, S., Grove, E.A., and Miller, R.J. (2005). The chemokine stromal cell-derived factor-1 regulates the migration of sensory neuron progenitors. *J. Neurosci.* 25, 3995–4003.

Bereiter-Hahn, J. (2005). Mechanics of crawling cells. *Med. Eng. Phys.* 27, 743–753.

Bereiter-Hahn, J., Strohmeier, R., Kunzenbacher, I., Beck, K., and Voth, M. (1981). Locomotion of *Xenopus* epidermis cells in primary culture. *J. Cell Sci.* 52, 289–311.

Betapudi, V., Licate, L.S., and Egelhoff, T.T. (2006). Distinct roles of nonmuscle myosin II isoforms in the regulation of MDA-MB-231 breast cancer cell spreading and migration. *Cancer Res.* 66, 4725–4733.

Blaser, H., Eisenbeiss, S., Neumann, M., Reichman-Fried, M., Thisse, B., Thisse, C., and Raz, E. (2005). Transition from non-motile behaviour to directed migration during early PGC development in zebrafish. *J. Cell Sci.* 118, 4027–4038.

Bleul, C.C., Farzan, M., Choe, H., Parolin, C., Clark-Lewis, I., Sordoski, J., and Springer, T.A. (1996). The lymphocyte chemoattractant SDF-1 is a ligand for LESTR/fusin and blocks HIV-1 entry. *Nature* 382, 829–833.

Brabletz, T., Jung, A., Spaderna, S., Hlubek, F., and Kirchner, T. (2005). Opinion: migrating cancer stem cells—an integrated concept of malignant tumour progression. *Nat. Rev. Cancer* 5, 744–749.

Bray, D., and White, J.G. (1988). Cortical flow in animal cells. *Science* 239, 883–888.

Burger, J.A., and Kipps, T.J. (2006). CXCR4: a key receptor in the crosstalk between tumor cells and their microenvironment. *Blood* 107, 1761–1767.

Chard, P.S., Bleakman, D., Christakos, S., Fullmer, C.S., and Miller, R.J. (1993). Calcium buffering properties of calbindin D28k and parvalbumin in rat sensory neurones. *J. Physiol.* 472, 341–357.

Charras, G.T., Yarrow, J.C., Horton, M.A., Mahadevan, L., and Mitchison, T.J. (2005). Non-equilibration of hydrostatic pressure in blebbing cells. *Nature* 435, 365–369.

Chew, T.L., Wolf, W.A., Gallagher, P.J., Matsumura, F., and Chisholm, R.L. (2002). A fluorescent resonant energy transfer-based biosensor reveals transient and regional myosin light chain kinase activation in lamella and cleavage furrows. *J. Cell Biol.* 156, 543–553.

Chisholm, R.L., and Firtel, R.A. (2004). Insights into morphogenesis from a simple developmental system. *Nat. Rev. Mol. Cell Biol.* 5, 531–541.

Doitsidou, M., Reichman-Fried, M., Stebler, J., Kopranner, M., Dorries, J., Meyer, D., Eguerra, C.V., Leung, T., and Raz, E. (2002). Guidance of primordial germ cell migration by the chemokine SDF-1. *Cell* 111, 647–659.

Dumstrei, K., Mennecke, R., and Raz, E. (2004). Signaling pathways controlling primordial germ cell migration in zebrafish. *J. Cell Sci.* 117, 4787–4795.

Furukawa, R., Maselli, A., Thomson, S.A., Lim, R.W., Stokes, J.V., and Fechheimer, M. (2003). Calcium regulation of actin crosslinking is important for function of the actin cytoskeleton in *Dictyostelium*. *J. Cell Sci.* 116, 187–196.

Gilmour, D., Knaut, H., Maischein, H.M., and Nusslein-Volhard, C. (2004). Towing of sensory axons by their migrating target cells in vivo. *Nat. Neurosci.* 7, 491–492.

Hauptmann, G., and Gerster, T. (1994). Two-color whole-mount in situ hybridization to vertebrate and *Drosophila* embryos. *Trends Genet.* 10, 266.

Henley, J., and Poo, M.M. (2004). Guiding neuronal growth cones using Ca<sup>2+</sup> signals. *Trends Cell Biol.* 14, 320–330.

Janson, L.W., and Taylor, D.L. (1993). In vitro models of tail contraction and cytoplasmic streaming in amoeboid cells. *J. Cell Biol.* 123, 345–356.

Jin, S.W., Beis, D., Mitchell, T., Chen, J.N., and Stainier, D.Y. (2005). Cellular and molecular analyses of vascular tube and lumen formation in zebrafish. *Development* 132, 5199–5209.

Jowett, T., and Lettice, L. (1994). Whole-mount in situ hybridizations on zebrafish embryos using a mixture of digoxigenin- and fluorescein-labelled probes. *Trends Genet.* 10, 73–74.

Kaksonen, M., Peng, H.B., and Rauvala, H. (2000). Association of cortactin with dynamic actin in lamellipodia and on endosomal vesicles. *J. Cell Sci.* 113, 4421–4426.

Kawakami, K., Takeda, H., Kawakami, N., Kobayashi, M., Matsuda, N., and Mishina, M. (2004). A transposon-mediated gene trap

- approach identifies developmentally regulated genes in zebrafish. *Dev. Cell* 7, 133–144.
- Kimmel, C., Ballard, W., Kimmel, S.R., Ullmann, B., and Schilling, T.F. (1995). Stages of embryonic development of the zebrafish. *Dev. Dyn.* 203, 253–310.
- Knaut, H., Werz, C., Geisler, R., and Nusslein-Volhard, C. (2003). A zebrafish homologue of the chemokine receptor Cxcr4 is a germ-cell guidance receptor. *Nature* 421, 279–282.
- Kovacs, M., Toth, J., Hetenyi, C., Malnasi-Csizmadia, A., and Sellers, J.R. (2004). Mechanism of blebbistatin inhibition of myosin II. *J. Biol. Chem.* 279, 35557–35563.
- Kunwar, P.S., Siekhaus, D.E., and Lehmann, R. (2006). In vivo migration: a germ cell perspective. *Annu. Rev. Cell Dev. Biol.* 22, 237–265.
- Kuo, J.C., Wang, W.J., Yao, C.C., Wu, P.R., and Chen, R.H. (2006). The tumor suppressor DAPK inhibits cell motility by blocking the integrin-mediated polarity pathway. *J. Cell Biol.* 172, 619–631.
- Köprunner, M., Thisse, C., Thisse, B., and Raz, E. (2001). A zebrafish nanos-related gene is essential for the development of primordial germ cells. *Genes Dev.* 15, 2877–2885.
- Langridge, P.D., and Kay, R.R. (2006). Blebbing of *Dictyostelium* cells in response to chemoattractant. *Exp. Cell Res.* 312, 2009–2017.
- Lapidot, T., Dar, A., and Kollet, O. (2005). How do stem cells find their way home? *Blood* 106, 1901–1910.
- Liou, J., Kim, M.L., Heo, W.D., Jones, J.T., Myers, J.W., Ferrell, J.E., Jr., and Meyer, T. (2005). STIM is a Ca<sup>2+</sup> sensor essential for Ca<sup>2+</sup>-store-depletion-triggered Ca<sup>2+</sup> influx. *Curr. Biol.* 15, 1235–1241.
- Luster, A.D., Alon, R., and von Andrian, U.H. (2005). Immune cell migration in inflammation: present and future therapeutic targets. *Nat. Immunol.* 6, 1182–1190.
- Marlow, F., Topczewski, J., Sepich, D., and Solnica-Krezel, L. (2002). Zebrafish Rho kinase 2 acts downstream of Wnt11 to mediate cell polarity and effective convergence and extension movements. *Curr. Biol.* 12, 876–884.
- Matsumura, F. (2005). Regulation of myosin II during cytokinesis in higher eukaryotes. *Trends Cell Biol.* 15, 371–377.
- Mejillano, M.R., Kojima, S., Applewhite, D.A., Gertler, F.B., Svitkina, T.M., and Borisy, G.G. (2004). Lamellipodial versus filopodial mode of the actin nanomachinery: pivotal role of the filament barbed end. *Cell* 118, 363–373.
- Moussavi, R.S., Kelley, C.A., and Adelstein, R.S. (1993). Phosphorylation of vertebrate nonmuscle and smooth muscle myosin heavy chains and light chains. *Mol. Cell. Biochem.* 127–128, 219–227.
- Murdoch, C. (2000). CXCR4: chemokine receptor extraordinaire. *Immunol. Rev.* 177, 175–184.
- Oberlin, E., Amara, A., Bachelier, F., Bessia, C., Virelizier, J.L., Arenzana-Seisdedos, F., Schwartz, O., Heard, J.M., Clark-Lewis, I., Legler, D.F., et al. (1996). The CXCR chemokine SDF-1 is the ligand for LESTR/fusin and prevents infection by T-cell-line-adapted HIV-1. *Nature* 382, 833–835.
- Paluch, E., Piel, M., Prost, J., Bornens, M., and Sykes, C. (2005). Cortical actomyosin breakage triggers shape oscillations in cells and cell fragments. *Biophys. J.* 89, 724–733.
- Paluch, E., Sykes, C., Prost, J., and Bornens, M. (2006). Dynamic modes of the cortical actomyosin gel during cell locomotion and division. *Trends Cell Biol.* 16, 5–10.
- Pechere, J.F., Derancourt, J., and Haiech, J. (1977). The participation of parvalbumins in the activation-relaxation cycle of vertebrate fast skeletal-muscle. *FEBS Lett.* 75, 111–114.
- Pollard, T.D., and Borisy, G.G. (2003). Cellular motility driven by assembly and disassembly of actin filaments. *Cell* 112, 453–465.
- Rafelski, S.M., and Theriot, J.A. (2004). Crawling toward a unified model of cell mobility: spatial and temporal regulation of actin dynamics. *Annu. Rev. Biochem.* 73, 209–239.
- Raucher, D., Stauffer, T., Chen, W., Shen, K., Guo, S., York, J.D., Sheetz, M.P., and Meyer, T. (2000). Phosphatidylinositol 4,5-bisphosphate functions as a second messenger that regulates cytoskeleton-plasma membrane adhesion. *Cell* 100, 221–228.
- Raz, E. (2003). Primordial germ-cell development: the zebrafish perspective. *Nat. Rev. Genet.* 4, 690–700.
- Raz, E., and Reichman-Fried, M. (2006). Attraction rules: germ cell migration in zebrafish. *Curr. Opin. Genet. Dev.* 16, 355–359.
- Reichman-Fried, M., Minina, S., and Raz, E. (2004). Autonomous modes of behavior in primordial germ cell migration. *Dev. Cell* 6, 589–596.
- Rhyner, J.A., Durussel, I., Cox, J.A., Ilg, E.C., Schafer, B.W., and Heizmann, C.W. (1996). Human recombinant alpha-parvalbumin and nine mutants with individually inactivated calcium- and magnesium-binding sites: biochemical and immunological properties. *Biochim. Biophys. Acta* 1313, 179–186.
- Roos, J., DiGregorio, P.J., Yeromin, A.V., Ohlsen, K., Lioudyno, M., Zhang, S., Safrina, O., Kozak, J.A., Wagner, S.L., Cahalan, M.D., et al. (2005). STIM1, an essential and conserved component of store-operated Ca<sup>2+</sup> channel function. *J. Cell Biol.* 169, 435–445.
- Sahai, E., and Marshall, C.J. (2003). Differing modes of tumour cell invasion have distinct requirements for Rho/ROCK signalling and extracellular proteolysis. *Nat. Cell Biol.* 5, 711–719.
- Sepich, D.S., Calmelet, C., Kiskowski, M., and Solnica-Krezel, L. (2005). Initiation of convergence and extension movements of lateral mesoderm during zebrafish gastrulation. *Dev. Dyn.* 234, 279–292.
- Shaner, N.C., Campbell, R.E., Steinbach, P.A., Giepmans, B.N., Palmer, A.E., and Tsien, R.Y. (2004). Improved monomeric red, orange and yellow fluorescent proteins derived from *Discosoma* sp. red fluorescent protein. *Nat. Biotechnol.* 22, 1567–1572.
- Sheetz, M.P., Sable, J.E., and Dobreiner, H.G. (2006). Continuous membrane-cytoskeleton adhesion requires continuous accommodation to lipid and cytoskeleton dynamics. *Annu. Rev. Biophys. Biomol. Struct.* 35, 417–434.
- Shohat, G., Shani, G., Eisenstein, M., and Kimchi, A. (2002). The DAP-kinase family of proteins: study of a novel group of calcium-regulated death-promoting kinases. *Biochim. Biophys. Acta* 1600, 45–50.
- Small, J.V., and Resch, G.P. (2005). The comings and goings of actin: coupling protrusion and retraction in cell motility. *Curr. Opin. Cell Biol.* 17, 517–523.
- Straight, A.F., Cheung, A., Limouze, J., Chen, I., Westwood, N.J., Sellers, J.R., and Mitchison, T.J. (2003). Dissecting temporal and spatial control of cytokinesis with a myosin II inhibitor. *Science* 299, 1743–1747.
- Strohmeier, R., and Bereiter-Hahn, J. (1984). Control of cell shape and locomotion by external calcium. *Exp. Cell Res.* 154, 412–420.
- Strohmeier, R., and Bereiter-Hahn, J. (1987). Hydrostatic pressure in epidermal cells is dependent on Ca-mediated contractions. *J. Cell Sci.* 88, 631–640.
- Svitkina, T.M., Verkhovskiy, A.B., McQuade, K.M., and Borisy, G.G. (1997). Analysis of the actin-myosin II system in fish epidermal keratocytes: mechanism of cell body translocation. *J. Cell Biol.* 139, 397–415.
- Taylor, D.L., Blinks, J.R., and Reynolds, G. (1980a). Contractile basis of amoeboid movement. VII. Aequorin luminescence during amoeboid movement, endocytosis, and capping. *J. Cell Biol.* 86, 599–607.
- Taylor, D.L., Wang, Y.L., and Heiple, J.M. (1980b). Contractile basis of amoeboid movement. VII. The distribution of fluorescently labeled actin in living amebas. *J. Cell Biol.* 86, 590–598.
- Torres-Vazquez, J., Gitler, A.D., Fraser, S.D., Berk, J.D., Van, N.P., Fishman, M.C., Childs, S., Epstein, J.A., and Weinstein, B.M. (2004). Semaphorin-plexin signaling guides patterning of the developing vasculature. *Dev. Cell* 7, 117–123.
- Totsukawa, G., Wu, Y., Sasaki, Y., Hartshorne, D.J., Yamakita, Y., Yamashiro, S., and Matsumura, F. (2004). Distinct roles of MLCK and ROCK in the regulation of membrane protrusions and focal adhesion dynamics during cell migration of fibroblasts. *J. Cell Biol.* 164, 427–439.
- Tsukita, S., and Yonemura, S. (1999). Cortical actin organization: lessons from ERM (ezrin/radixin/moesin) proteins. *J. Biol. Chem.* 274, 34507–34510.
- Ulrich, F., Krieg, M., Schotz, E.M., Link, V., Castanon, I., Schnabel, V., Taubenberger, A., Mueller, D., Puech, P.H., and Heisenberg, C.P. (2005). Wnt11 functions in gastrulation by controlling cell cohesion through Rab5c and E-cadherin. *Dev. Cell* 9, 555–564.

- Van Haastert, P.J., and Devreotes, P.N. (2004). Chemotaxis: signaling the way forward. *Nat. Rev. Mol. Cell Biol.* 5, 626–634.
- Verkhovskiy, A.B., Svitkina, T.M., and Borisy, G.G. (1995). Myosin II filament assemblies in the active lamella of fibroblasts: their morphogenesis and role in the formation of actin filament bundles. *J. Cell Biol.* 131, 989–1002.
- Verkhovskiy, A.B., Svitkina, T.M., and Borisy, G.G. (1999). Self-polarization and directional motility of cytoplasm. *Curr. Biol.* 9, 11–20.
- Vicente-Manzanares, M., Webb, D.J., and Horwitz, A.R. (2005). Cell migration at a glance. *J. Cell Sci.* 118, 4917–4919.
- Wadgaonkar, R., Nurmukhambetova, S., Zaiman, A.L., and Garcia, J.G. (2003). Mutation analysis of the non-muscle myosin light chain kinase (MLCK) deletion constructs on CV1 fibroblast contractile activity and proliferation. *J. Cell. Biochem.* 88, 623–634.
- Weed, S.A., Karginov, A.V., Schafer, D.A., Weaver, A.M., Kinley, A.W., Cooper, J.A., and Parsons, J.T. (2000). Cortactin localization to sites of actin assembly in lamellipodia requires interactions with F-actin and the Arp2/3 complex. *J. Cell Biol.* 151, 29–40.
- Weidinger, G., Wolke, U., Kopranner, M., Klinger, M., and Raz, E. (1999). Identification of tissues and patterning events required for distinct steps in early migration of zebrafish primordial germ cells. *Development* 126, 5295–5307.
- Weidinger, G., Wolke, U., Kopranner, M., Thisse, C., Thisse, B., and Raz, E. (2002). Regulation of zebrafish primordial germ cell migration by attraction towards an intermediate target. *Development* 129, 25–36.
- Westerfield, M. (1995). *The Zebrafish Book* (Oregon: University of Oregon Press).
- Wolf, K., Mazo, I., Leung, H., Engelke, K., von Andrian, U.H., Deryugina, E.I., Strongin, A.Y., Brocker, E.B., and Friedl, P. (2003). Compensation mechanism in tumor cell migration: mesenchymal-amoeboid transition after blocking of pericellular proteolysis. *J. Cell Biol.* 160, 267–277.
- Xu, J., Wang, F., Van Keymeulen, A., Herzmark, P., Straight, A., Kelly, K., Takuwa, Y., Sugimoto, N., Mitchison, T., and Bourne, H.R. (2003). Divergent signals and cytoskeletal assemblies regulate self-organizing polarity in neutrophils. *Cell* 114, 201–214.
- Yamada, A., Hirose, K., Hashimoto, A., and Iino, M. (2005). Real-time imaging of myosin II regulatory light-chain phosphorylation using a new protein biosensor. *Biochem. J.* 385, 589–594.
- Yamaguchi, H., Wyckoff, J., and Condeelis, J. (2005). Cell migration in tumors. *Curr. Opin. Cell Biol.* 17, 559–564.
- Yanai, M., Kenyon, C.M., Butler, J.P., Macklem, P.T., and Kelly, S.M. (1996). Intracellular pressure is a motive force for cell motion in *Amoeba proteus*. *Cell Motil. Cytoskeleton* 33, 22–29.
- Yoon, C., Kawakami, K., and Hopkins, N. (1997). Zebrafish vasa homologue RNA is localized to the cleavage planes of 2- and 4-cell-stage embryos and is expressed in the primordial germ cells. *Development* 124, 3157–3165.
- Zhang, S.L., Yu, Y., Roos, J., Kozak, J.A., Deerinck, T.J., Ellisman, M.H., Stauderman, K.A., and Cahalan, M.D. (2005). STIM1 is a  $Ca^{2+}$  sensor that activates CRAC channels and migrates from the  $Ca^{2+}$  store to the plasma membrane. *Nature* 437, 902–905.
- Zlotnik, A. (2006). Involvement of chemokine receptors in organ-specific metastasis. *Contrib. Microbiol.* 13, 191–199.